Carbon 205 (2023) 345–352

Contents lists available at ScienceDirect

Carbon

journal homepage: www.elsevier.com/locate/carbon

Capillary adhesion governs the friction behavior of electrochemically corroded polycrystalline diamond

Chen Xiao [a,b], Liang Peng [b], Cyrian Leriche [a,b], Feng-Chun Hsia [a], Bart Weber [a,b], Steve Franklin [a,c,*]

[a] Advanced Research Center for Nanolithography (ARCNL), Science Park 106, 1098XG, Amsterdam, the Netherlands
[b] Van der Waals-Zeeman Institute, Institute of Physics, University of Amsterdam, Science Park 904, 1098XH, Amsterdam, the Netherlands
[c] Department of Mechanical Engineering, The University of Sheffield, Sheffield, S13JD, UK

ARTICLE INFO

Keywords:
Electrochemically corroded diamond
Capillary force
Frictional force
Surface oxidation
Boundary element method
Atomic force microscopy

ABSTRACT

The friction behavior of rough polycrystalline diamond (PCD) surfaces is important in many applications and devices that are required to operate in various harsh environments and it can be argued that a thorough understanding of the friction behavior is essential to the application performance. However, the interplay between electrochemical corrosion, capillary adhesion and friction behavior of PCD in multi-asperity contacts is still poorly understood. In this work, we quantify the interfacial capillary adhesion at contact interfaces and its effect on the friction response, between a colloidal microsphere and rough PCD films before and after electrochemical corrosion, for water-immersed, low RH, and humid air conditions. For these multi-asperity contacts, we demonstrate how electrochemical corrosion influences the surface hydrophilicity of the PCD surfaces, and how capillary adhesion due to water condensation contributes to the friction force. We estimate the capillary forces from both the microscopic lateral force experiments and elastoplastic boundary element method (BEM) contact calculations. The combined results indicate strongly that the observed increase in friction force on electrochemically-corroded PCD surfaces is governed by enhanced capillary adhesion at the contact interface, as affected by surface hydrophilicity and environmental humidity.

1. Introduction

Due to excellent mechanical properties, wear and corrosion resistance, high thermal stability and chemical inertness, polycrystalline diamond (PCD) is an attractive candidate for applications and devices operating in a variety of harsh environments [1,2]. PCD is currently utilized in various extreme wear and corrosion applications such as orthopedic artificial joint prostheses and heart valves in the human body [3–5], mechanical seals and bearings in marine ships [6], micro-/nano-electromechanical systems (MEMS/NEMS) [7,8], coatings for alloys used in nuclear facilities [9], etc. Sustained operation in corrosive environments leads to physical and chemical changes to the PCD surface, resulting in changes to the tribological behavior that could potentially affect the working performance and service lifetime. Nevertheless, the interplay between electrochemical corrosion, capillary adhesion and friction behavior of PCD in multi-asperity contacts is still poorly understood.

Friction is a system property, depending not only on the intrinsic properties of the contacting materials, but also on the extrinsic parameters of the sliding environment. Interfacial capillary condensation can play an important role, occurring below the saturation vapor pressure as a result of increased van der Waals interactions inside the confined space of asperity contacts, and inducing capillary bridges with a negative curvature in the direction normal to the interface [10]. The Laplace pressure difference inside and outside the meniscus bridge leads to capillary adhesion, which strongly impacts the friction behavior across scales [11]. The influence of capillary condensation on the contact mechanics and friction behavior at nano-asperity contacts has been widely studied in the literature [12–14]. The thickness and structure of water adsorption on contacting surfaces, which is governed by surface hydrophilicity and ambient humidity (RH) [15,16], plays a significant role in the friction behavior. In previous work concerning single-asperity contact between hydrophilic surfaces, the interfacial adhesion/pull-off force value was added directly to the applied normal load and considered to be responsible for the change in friction force [17–19]. This interpretation has also been successfully extended to smooth

---

[*] Corresponding author. Advanced Research Center for Nanolithography (ARCNL), Science Park 106, 1098XG, Amsterdam, the Netherlands.
E-mail address: s.franklin@arcnl.nl (S. Franklin).

https://doi.org/10.1016/j.carbon.2023.01.050
Received 21 October 2022; Received in revised form 8 January 2023; Accepted 24 January 2023

multi-asperity contacts where the interfacial gap is completely filled by the meniscus bridge due to water condensation, so that in this case the capillary adhesion is independent of the actual solid-solid contact area [20]. However, when the surface roughness is larger than the adsorbed water thickness, the capillary adhesion shows strong real solid-solid contact area dependence because the interfacial gap is not filled by the condensed water meniscus [13,21,22]. Few studies have considered how capillary adhesion, in a microscopic multi-asperity contact with a relatively rough PCD surface, influences the interfacial friction behavior.

A diamond surface is naturally terminated by heteroatoms, such as hydrogen or oxygen. H-terminated diamond can be converted to O-terminated through surface oxidation induced by electrochemical corrosion in an aqueous electrolyte solution [23,24]. Moreover, surface modification by chemical corrosion also leads to changes in surface structure and chemistry. X-ray photoelectron spectroscopy (XPS) and Raman spectroscopy have shown evidence for the corrosion proceeding via an oxidation reaction, which occurs more strongly at the grain boundaries, leading to an increase in carbon sp^2 content and the formation of oxides of C═O, C–O/OH, and C(═O)–OH on the corroded surface [25,26]. The changes in surface hydrophilicity and interfacial shear strength due to these surface modifications contribute to changes in the friction response of the tribological system [27]. In addition, the anisotropic corrosion characteristics of the diamond crystal may alter the surface topography [28], which will affect the contact dynamics and associated interfacial interactions. A quantitative analysis of the contribution of the corrosion-dependent capillary adhesion to friction at corroded PCD interfaces would not only help to understand the changes in tribological performance of PCD devices during environmental aging/oxidation, but would also provide a valuable paradigm of the surface chemistry effect on nanoscale friction behavior.

In this work, we show how electrochemical corrosion influences the surface hydrophilicity of microcrystalline diamond (MCD) and nanocrystalline diamond (NCD) surfaces, and how capillary adhesion due to water condensation contributes to friction force at multi-asperity contacts, on pristine and corroded diamond surfaces in low RH air, humid air, and water-immersed conditions. To quantify the capillary adhesion at the contact interfaces and its effect on the friction response, the areas of solid contact and the capillary-wetted areas at multi-asperity interfaces are estimated using elastoplastic boundary element method (BEM) contact calculations based on the interfacial gaps as affected by the ambient humidity and the surface hydrophilicity.

2. Experimental

2.1. Materials

Undoped MCD and NCD films produced by Advanced Diamond Technologies (Romeoville, USA) with a thickness of 1 μm, synthesized by hot filament CVD on a single crystal p-silicon substrate with a square area of 40 mm × 40 mm, were adopted as the working electrodes in electrochemical tests. The (root mean square, RMS) surface roughness and grain size of the non-corroded diamond films were measured in tapping mode by atomic force microscopy (AFM) to be approximately 13.2 nm and 200–500 nm for MCD, and 10.4 nm and 50–100 nm for NCD respectively, over a square scanned area of 2 μm × 2 μm using a sharp Si AFM tip (RTESPA-300, Bruker) with a nominal diameter of approximately 20 nm. The sample surfaces were cleaned using chemically pure ethanol (Sigma Aldrich) and subsequently deionized water, and dried using pure N_2 gas before performing the electrochemical tests and lateral force measurements.

2.2. Electrochemical corrosion

All electrochemical and topographical experiments were performed at room temperature (22 °C). As illustrated in Fig. 1a and b, the MCD and NCD samples were mounted in an AFM-compatible electrochemical cell module (Dimension Icon, Bruker, MA, USA): the diamond-coated side was in contact with two gold-plated spring pins that provided the electrical connection with the working electrode. A circular area of 35 mm diameter on the sample surface was exposed to an electrolyte solution of 0.1 M potassium chloride (KCl, Sigma Aldrich) for different corrosion durations, and a fluorine rubber O-ring was used to seal the gap between the sample clamp and sample [29]. Open circuit potential (OCP) and chronoamperometry measurements were performed using an electrochemical workstation with a bipotentiostat (CHI 760E, CH Instruments, TX, USA). Ag|AgCl and Pt wires served as the reference and counter electrodes respectively and all potentials are given with reference to the reference electrode (Ag|AgCl in 0.1 M KCl). An anodic (oxidative) potential of 2.5 V was applied to the MCD and NCD samples in electrochemical corrosion tests.

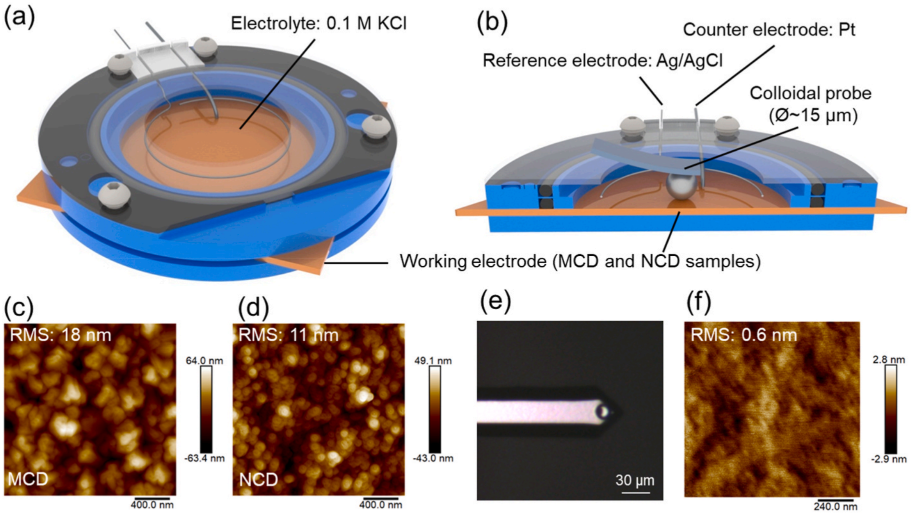

Fig. 1. Schematic of electrochemical-atomic force microscopy (EC-AFM) set-up: (a) isometric view and (b) cutaway view. AFM images of pristine (c) MCD and (d) NCD surfaces. (e) Optical image of colloidal probe with a diameter of 15 μm. (f) AFM image of the apex of the microsphere. (A colour version of this figure can be viewed online.)

2.3. Lateral force measurements on non-corroded and corroded MCD and NCD surfaces

To assess the influence of electrochemical corrosion on the friction behaviors of MCD and NCD surfaces, lateral force measurements were conducted on non-corroded and corroded samples using AFM equipped with a semi-open fluid cell (Fig. 1b) in humid air (~50% RH), low humidity (10%–20% RH), and water liquid immersed conditions. The gas environments were established by controlling the flow rates of water-saturated N_2 and dry N_2. To obtain a steady-state gas mixture in the fluid cell, at least 30 min equilibration time was introduced before every lateral force measurement. A silica microsphere with a diameter of 15 μm, attached to a silicon cantilever with a spring constant of approximately 45 N/m, was used to measure the lateral force with a stroke length of 100 nm (Fig. 1e). The surface topography of the apex of the silica microsphere was estimated by scanning a test grating with a known tip curvature of 10 nm (TGT1, Tipsnano, Estonia). In this way, the RMS roughness of the silica microsphere was estimated at approximately 0.6 nm over a sampling area of 1.2 μm × 1.2 μm. The torsional stiffness of the silica probe was calibrated as approximately 27 μN/V using trapezoidal gratings (TGF11, Mikro Masch, Germany). During all the experiments, the ambient temperature was maintained at 23 ± 2 °C, and a sliding velocity of 2 μm/s was used.

3. Results and discussion

3.1. Electrochemical corrosion of MCD and NCD

Chronoamperometry measurements with an applied voltage of 2.5 V in a 0.1 M KCl electrolyte solution were performed on MCD and NCD surfaces using EC-AFM. The surface topography at the microscale was imaged in-situ at various electrochemical corrosion durations using a sharp Si tip with a radius of 10 nm. Fig. 2a and b shows the AFM images obtained on MCD and NCD surfaces before and after corrosion for increasing time, together with images of the static water contact angles. No significant difference between the RMS surface roughness of non-corroded and corroded diamond surfaces was observed (Fig. 2c). Five randomly selected locations on non-corroded and corroded diamond surfaces were scanned ex-situ, and shows the same trend as the results of Fig. 2c, as displayed in Fig. S1 in the supplementary information. However, the water contact angle of both MCD and NCD surfaces was shown to decrease significantly, demonstrating that the surfaces became more hydrophilic after electrochemical corrosion. These results suggest that the predominant effect of the electrochemical corrosion process is to alter the surface chemistry of the topmost layers of the diamond films, through oxidation, without changing the surface topography, at least down to the length scale accessible using a 10 nm radius AFM tip. A previous Raman and XPS study indicated that a thin surface layer of carbon on the MCD and NCD is oxidized upon exposure to a corrosive environment [30]. As shown in Fig. S2 in the supplementary information, compared to the non-corroded diamond surface, a small increase in the D band region (~1360 cm^{-1}) of the Raman spectra of corroded MCD and NCD diamond surfaces indicated that the diamond films were oxidized during electrochemical corrosion. This is also supported by EDX characterization, which showed an increased oxygen signal on the corroded diamond surfaces (Fig. S3). To qualitatively determine the effect of the electrochemical corrosion on the chemical composition of the uppermost surface, XPS was performed on non-corroded and corroded MCD and NCD surfaces. With corrosion, an increase in oxygen, silicon, and chlorine species was evident (Table S1). In the detailed C 1s spectra for MCD (Table S2) both lower (sp^2) and higher (C–O, C═O) binding energy species were observed after corrosion, suggesting the formation of sp^2-type and oxidized carbon species as a result of the corrosion process. The C 1s spectra of NCD showed a similar trend but this does not provide sufficient basis for a reliable interpretation by peak fitting due to the broad characteristic peaks. The oxidation reactions that occur on diamond surfaces are stimulated electrochemically and this leads to an increase in oxygen species and increased wetting of the diamond surfaces.

3.2. Tribological responses of non-corroded and electrochemically corroded MCD/NCD surfaces

To investigate the effect of electrochemical corrosion on the tribological responses of the MCD and NCD surfaces, lateral force measurements under different applied normal loads were performed using a silica colloidal microsphere in water-immersed, low RH, and humid air conditions, as shown in Fig. 3. The friction coefficients for the different cases were calculated by linear fitting of the friction force (F_f) as a function of normal load, and are compared in Fig. 4. In the immersion condition, there is little observable difference between the friction coefficients measured on MCD and NCD surfaces in the non-corroded and corroded conditions. Any small differences in friction coefficient may be attributed to the combined effects of surface topography and the surface hydrophilicity-dependent boundary lubrication. Compared to MCD, the slightly higher coefficients of friction observed for the NCD surface are likely due to slightly larger real contact areas resulting from the relative smoothness of the NCD, which is supported by the BEM calculations (see Figs. 6a and 7c). In addition, after electrochemical corrosion, both the MCD and NCD surfaces become more hydrophilic and, in water-immersed conditions, it is known that higher hydrophilicity leads to a reduction in friction [31,32].

The friction coefficients increase significantly from 'water-immersed' to 'low RH' and then again to 'humid air' conditions. This

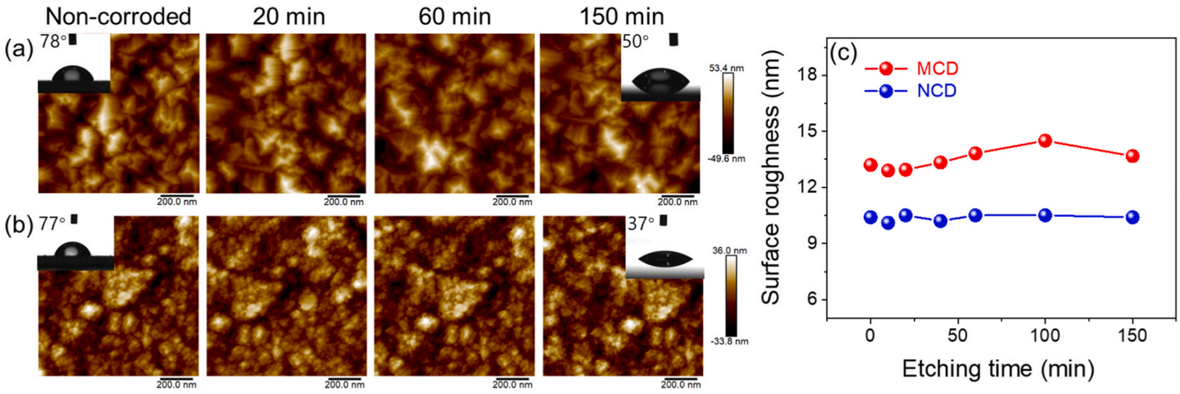

Fig. 2. In-situ AFM imaging with the scanning area of 2 μm × 2 μm illustrating the surface topography evolution of MCD (a) and NCD (b) at various electrochemical corrosion time. Insets show the images of the static water contact angle of MCD and NCD surfaces before and after 2.5 h electrochemical corrosion (c) Surface roughness (RMS) of the measured area in (a) and (b). (A colour version of this figure can be viewed online.)

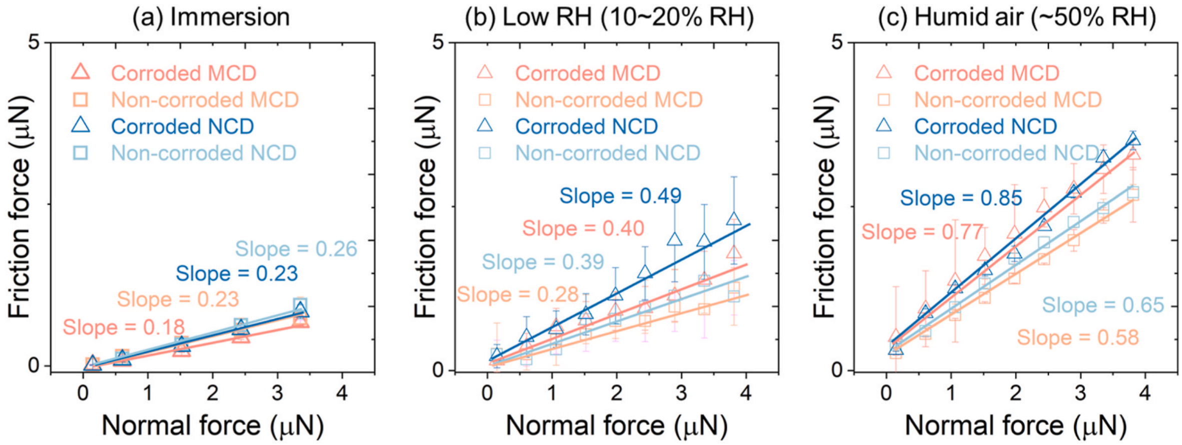

Fig. 3. Friction forces against a 15 μm diameter silica colloidal sphere, as a function of applied normal forces, measured in (a) water immersion, (b) low RH, and (c) humid air conditions for MCD and NCD surfaces before and after 2.5 h electrochemical corrosion. (A colour version of this figure can be viewed online.)

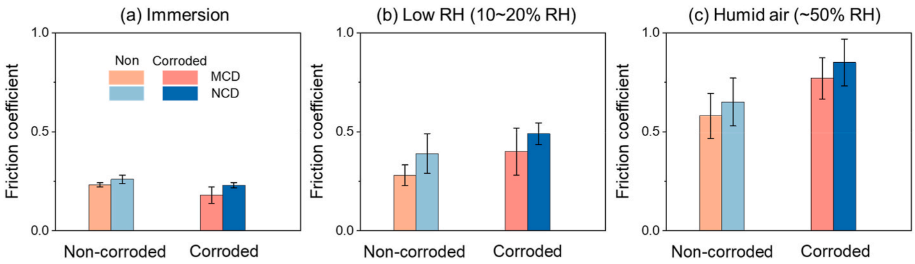

Fig. 4. Friction coefficients against a 15 μm diameter silica colloidal sphere, measured in (a) water immersion, (b) low RH, and (c) humid air conditions for MCD and NCD surfaces before and after 2.5 h electrochemical corrosion. (A colour version of this figure can be viewed online.)

suggests that the effect of capillary forces on the normal force, which is not present in the water-immersed condition, is already significant in air at low relative humidity of ~10–20%, then increases even more at the higher relative humidity of ~50%. In ambient air conditions, corroded surfaces with higher hydrophilicity result in larger friction forces because more hydrophilic surfaces are more favorable for water condensation at the contact interface [33], thus the total area over which the Laplace pressure acts, A_{cap}, increases, which increases the capillary force F_{cap}.

$$F_{cap} = P_{Laplace} \times A_{cap}. \tag{1}$$

Qualitatively, A_{cap} is also increased by increasing the RH, resulting in a higher capillary adhesive force that provides an additional normal load and thus increased friction when the surfaces are in contact [34].

3.3. Contribution of capillary interfacial adhesion to friction behavior

The friction results suggest that the effect of capillary forces on the normal force is significant and depend strongly on the environmental humidity. In an initial attempt to gain insight into the magnitude of these forces, AFM pull-off force measurements were carried out between the colloidal sphere and MCD/NCD surfaces under different environmental conditions. The forces measured were very low and similar for MCD and NCD diamond surfaces, see Fig. S4 in Supplementary Information. Nevertheless, for both materials a slight increase in pull-off force was observed for the corroded condition compared to non-corroded in the low RH and humid air environments, which can be attributed to the greater hydrophilicity of the corroded diamond surfaces (see Fig. 2): as mentioned previously, a greater hydrophilicity promotes vapor condensation and an increase in A_{cap}, thus an increase in the capillary force acting over the capillary-wetted area [33,35,36].

The pull-off adhesion forces shown in Fig. S4 were determined from the $f-d$ curves and based on the maximum deflection of the cantilever in the attractive region, just before the tip snap-off to the freestanding position. At this point there is no applied normal load at the solid interfaces and only minimal contact between the relatively smooth surface of the colloidal microsphere and a few asperities on the MCD and NCD surfaces at the interface. Under such circumstances, the measured pull-off force cannot be expected to reliably reflect the interfacial adhesion force under loaded conditions during interfacial sliding in a rough multi-asperity contact. This is an example of the phenomenon known as the "adhesion paradox" [37,38].

Direct measurement of adhesion under loading conditions remains very challenging and is one of the barriers to achieving a true understanding of friction in microscopic multi-asperity contacts. In order to estimate the contribution of capillary adhesion to friction in such contacts, the capillary adhesion force can be estimated using the following force balance [39]:

$$|F_{total}| = |F_{elastic}| = |F_{ex}| + |F_{cap}| \tag{2}$$

where the sum of the capillary adhesion force (F_{cap}) and the externally applied load (F_{ex}) represents the total normal force F_{total}, which balances the elastic force ($F_{elastic}$) generated by compressed asperities at the interface. When the colloidal sphere-diamond contact is fully immersed in water, the capillary adhesion force is negligible because capillary menisci can only form in the gas phase. The results given in Fig. 3 indicate that the friction force is approximately proportional to the normal force. If we assume that any additional lubrication effect in the case of immersion can be neglected and that the capillary force deforms the contacting interface in the same way as the applied force, so that the increase in friction force from low RH ('dry') to higher RH ('humid') originates entirely from the capillary force, the reduction in friction in the immersed state can be used to estimate the capillary adhesive force [11,34]:

$$\mathrm{COF}_{\mathrm{ambient}} = \mathrm{COF}_{\mathrm{immersed}} \times (1 + F_{\mathrm{cap}}/F_{\mathrm{ex}}), \tag{3}$$

Where $\mathrm{COF}_{\mathrm{ambient}}$ and $\mathrm{COF}_{\mathrm{immersed}}$ are the COF measured in ambient and immersed environments, respectively. Taking the applied normal load of 2 μN as an example, the total normal load and capillary force component on corroded MCD and NCD surfaces in different environmental conditions are given in Table S3 in the Supplementary Information.

The elastic and capillary forces acting at multi-asperity interfaces can also be estimated numerically using BEM, which is a numerical computational method of solving linear partial differential equations which have been formulated as integral elasticity equations [40]. In this case the calculation consists of two parts: contact calculations based on the BEM [41] and calculations of the area wetted by the capillary liquid (A_{cap}) of diamond surfaces [34]. The surface topography measured by AFM, of corroded MCD and NCD films and the colloidal microsphere, were adopted in the BEM calculation as input together with the mechanical properties (i.e., hardness and elastic modulus) listed in Table S4 [42]. Fig. 5 displays the BEM calculated results and shows how the topography is elastoplastically deformed by a given load (F_{total}) in the absence of adhesion. The resulting interface gap profile can be used to estimate the solid-solid contact area and the capillary area associated with that interface geometry. We assume here that water can condense at regions of the interface within which the interfacial gap is smaller than W,

$$W = 2h + d_c, \tag{4}$$

where h is the equilibrium thickness of the adsorbed water layer and d_c (= 1.5 nm for 20% RH and 3 nm for 50% RH) is the critical distance for capillary condensation on a silicon surface [35]. However, since the water adsorption behavior on electrochemically corroded diamond surfaces is unknown, W is calculated here assuming values from the literature for a *hydrophilic silicon* surface that correspond to a water partial pressure (P/P_{sat}) of 10%–20% RH for dry ($h = 0.5$ nm) and 50% RH for humid air ($h = 1.3$ nm) conditions [35,43]. In Fig. 5b–d for an electrochemically corroded MCD film and Fig. 5f–h for an electrochemically corroded NCD film, the blue areas represent the solid-solid contact area with an interface gap smaller than 0.2 nm and the white regions represent the estimated capillary area with an interface gap smaller than W. The correlation between the measured friction coefficient, which was constant for all applied normal forces within the range 0.2–3.8 μN, and the calculated real solid contact area A_{solid} of corroded MCD and NCD surfaces at an applied normal force of 2 μN, under different environmental conditions, is shown in Fig. 6a. According to Bowden and Tabor's simple theory of adhesive friction [44], the friction force is proportional to the real contact area (A_{solid}) and the shear strength (τ) of two contacting surfaces [45],

$$F_f = \tau \cdot A_{\mathrm{solid}}. \tag{5}$$

It can be expected that the electrochemical corrosion results in a decrease in τ because of the relatively low hardness and shear strength, compared to diamond, of the corrosion product formed on the diamond surface. This would result in a reduction of the friction coefficient, which is not observed experimentally. Indeed, the very good correlation between measured friction coefficient and calculated real solid contact area indicates that the increase in A_{solid} dominates the friction behavior. Thus, for a given externally-applied load on a corroded diamond surface, the increase in A_{solid} with increasing ambient humidity originates predominantly from the enhanced capillary effect at the contacting interfaces, which pulls the colloidal microsphere downwards and increases the load (eq. (2)), resulting in higher friction during the sliding process.

To quantitatively analyze the capillary contribution to the increased normal load which increases the friction force when relative motion occurs, the capillary force can be expressed by the Laplace pressure difference within the interfacial area wetted by a condensed meniscus,

$$P_{\mathrm{Laplace}} = \frac{R_g T}{V} \ln\left(\frac{P}{P_{sat}}\right) \tag{6}$$

where V the molar volume of water, R_g the ideal gas constant, T the temperature, P the partial vapor pressure of ambient environment, and P_{sat} the saturated vapor pressure. The capillary force is then given by the Laplace pressure acting over the whole capillary area A_{cap} (total area of blue and white patches in Fig. 5) [46],

$$F_{cap} = P_{\mathrm{Laplace}} \times A_{cap} = \frac{R_g T}{V} \ln\left(\frac{P}{P_{sat}}\right) \times A_{cap} \tag{7}$$

Fig. 6b compares the capillary force values estimated by the friction experiments (Fig. 4 and eq. (3)) with the BEM calculation (Fig. 5 and eq. (7)) for a colloidal microsphere on corroded MCD and NCD surfaces with an applied normal load of 2 μN in air at low RH and humid.

The results in Fig. 6b show that the capillary forces estimated in both ways show the same trend to increase as the humidity increases, but that the BEM calculated values are consistently lower than the experimentally estimated values. Four main factors may contribute to this inconsistency:

1. In the BEM calculation, reference values for the equilibrium thickness h of the adsorbed water layer and the critical distance d_c for capillary condensation are taken from the literature for a hydrophilic *silicon* surface rather than for diamond, for which these values are unknown. In addition, the literature values for silicon were measured using attenuated total reflection infrared spectroscopy, which is very sensitive to the sample preparation and measurement environment. These measurements must therefore be considered to be of low

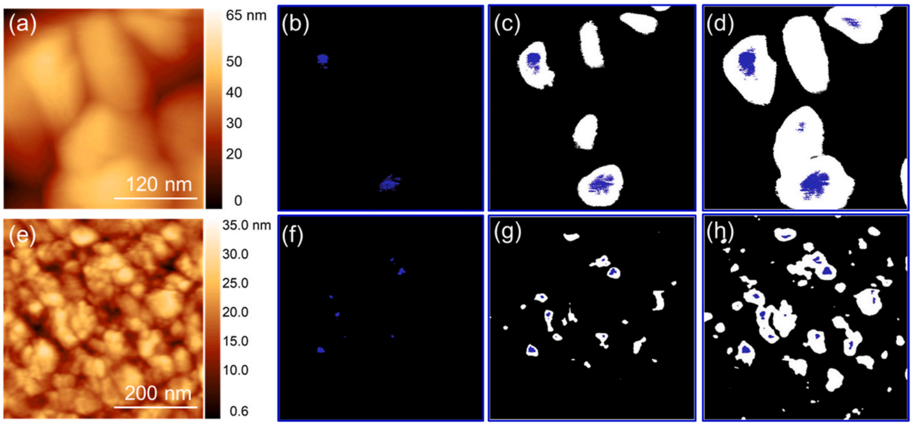

Fig. 5. Colloidal sphere on corroded diamond contact calculation using BEM (MCD: a-d; NCD: e-h). AFM images of corroded MCD (a) and NCD (e). Simulating the contact status in immersion (b, f), dry (c, g), and humid air (d, h) condition under the load of F_{total} shown in Table S3, the solid contact area (blue patches) and capillary-wetted area (white patches) were calculated by the Tribology Simulator based on the topography of the colloid microsphere used in the experiments as measured by AFM (Fig. 1f). (A colour version of this figure can be viewed online.)

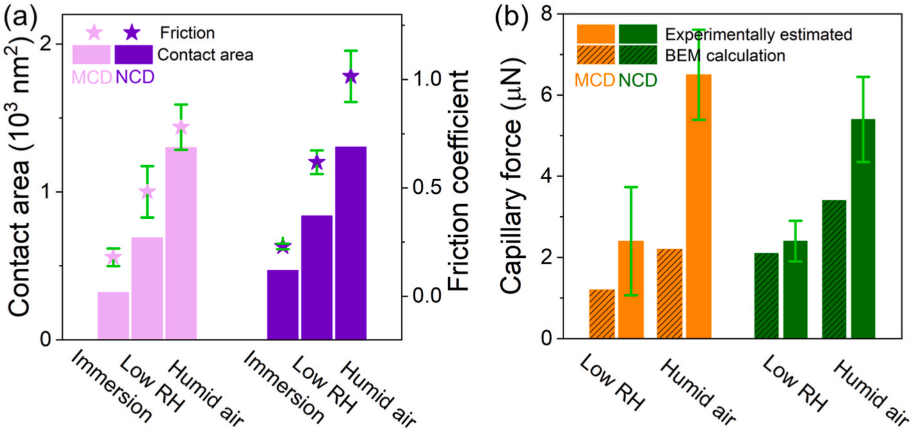

Fig. 6. (a) Correlation between real contact area estimated by BEM contact calculations (blue regions in Fig. 5b–d and 5f-h) and friction coefficients of corroded MCD and NCD surfaces in immersion, low RH, and humid air conditions. (b) Comparison of capillary forces calculated by experimental results (Fig. 4) and BEM calculations (Fig. 5) of colloid microsphere on MCD and NCD surfaces in low RH and humid air conditions. (A colour version of this figure can be viewed online.)

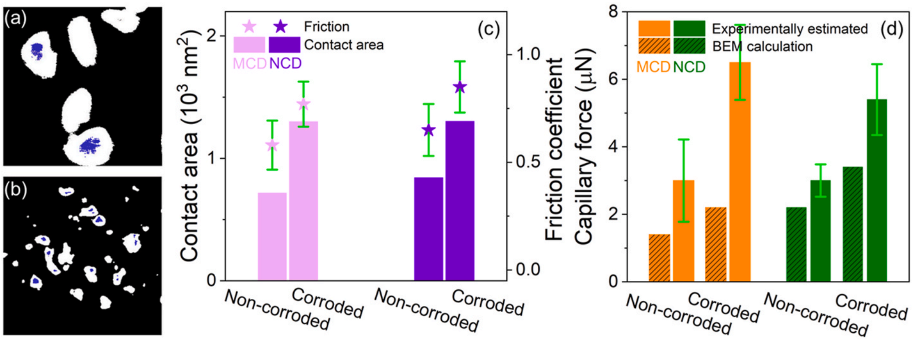

Fig. 7. Colloidal sphere on pristine diamond contact calculation. Simulating the contact status of MCD (a) and NCD (b) in humid air condition under the load of F_{total} shown in Table S5, the solid contact area (blue patches) and capillary-wetted area (white patches) were calculated by the Tribology Simulator based on the topography of the colloid microsphere (Fig. 1f) and PCD films (Fig. 5a and e) used in the experiments as measured by AFM. (c) Correlation between real contact area estimated by BEM contact calculations (blue patches in a and b) and friction coefficients of non-corroded and corroded MCD and NCD surfaces in humid air. (d) Comparison of capillary forces calculated by experimental results (Fig. 4) and BEM calculations of colloidal microsphere on non-corroded and corroded MCD and NCD surfaces in humid air. (A colour version of this figure can be viewed online.)

precision. Moreover, the possible solid-like structure of the adsorbed water layer, with different hydrogen bonding interactions, was not considered in this study. Such a structure would increase the capillary adhesion and further increase the friction force [47].

2. In the BEM calculation, a static contacting condition was assumed for the capillary condensation. However, under the dynamic sliding conditions of the experiments, the capillary necks encapsulating the multi-asperity nanocontacts are forced to grow to a more elongated shape, thus increasing d_c and even facilitating the merging of the adjacent liquid bridges [48]. This would mean that A_{cap} is greater than estimated by the BEM calculation and that the capillary force calculated by eq. (7) is an under-estimation.
3. The experimental estimate shown in Fig. 6b indicates that the capillary force acting at the silica-diamond interface, at least for humid air conditions, is greater than the externally-applied force, which was up to 4 μN. In this case the interface may be in the ‘sticky’ regime, in which F_{cap} may increase more rapidly with decreasing separation than F_{total} [38]. The latter would mean that eq. (3) is invalid, and the discrepancy between the experimentally estimated and BEM calculated capillary forces may then be due to an imprecise value of F_{total}.
4. The possibility of an additional boundary lubrication effect due to the confined adsorbed water film on hydrophilic contact surfaces is neglected in eq. (3) [48]. This would lead to underestimation of the friction force in the immersed condition, and thus overestimation of the capillary effect using eq. (3) for humid air conditions.

In summary, although the experimentally-estimated and BEM-estimated calculations for capillary forces show similar trends with increasing relative humidity, there are a number of possible reasons why the absolute values calculated are imprecise and not comparable.

The surface hydrophilicity also plays a critical role in the water adsorption isotherm and thus influences the formation of water menisci around asperity contacts. A pristine (i.e., non-corroded) diamond surface is terminated mainly by C–H groups and our results (Fig. 2) show that it had a water contact angle of approximately 78° [49]. During electrochemical corrosion treatment, polycrystalline diamond surfaces, and especially their intercrystallite boundaries [30], are oxidized to give O-terminations (C–O–C, C=O or C–O groups), resulting in a significant increase in surface hydrophilicity. Generally, a hydrophilic surface with high surface energy facilitates vapor adsorption and dynamic capillary wetting [50]. For this reason, for the same environmental condition, corroded diamond surfaces exhibit greater friction than pristine samples due to the greater capillary condensation and A_{cap}. To investigate the capillary force change and its contribution to the increased friction response after electrochemical corrosion, the capillary force at the interface of a colloidal microsphere and pristine polycrystalline diamond surfaces were estimated by friction force experiments and BEM calculations as described previously. In this case, the water adsorption isotherm on *hydrophobic* silicon surface was used for the BEM calculations, again because the data for pristine polycrystalline diamond is unknown. For hydrophobic silicon, the average thickness value of the adsorbed water layer is about 0.2 nm, yielding a W value of 3 nm at 20% RH and 4.5 nm at 50% RH [51]. Fig. 7a (MCD) and 7b (NCD) display the solid contact area (blue patches) and capillary-wetted area (white patches) estimated by BEM calculation for the F_{total} given in Table S5. As discussed earlier for Fig. 6a (in which corroded samples are compared for different environments) there is good correlation between the measured friction coefficient and calculated real solid contact area in Fig. 7c. For the humid air condition, the interfacial capillary adhesion values obtained from eq. (7) are compared with the experimentally estimated values (Table S5) in Fig. 7d. The results suggest that the increase in surface hydrophilicity resulting from the electrochemical corrosion gave a significant enhancement of the interfacial capillary adhesion. After 2.5 h electrochemical corrosion, for MCD the water contact angle of the diamond film decreased from 78° to 50° whilst the capillary force obtained by BEM calculation increased from 1.4 μN to 2.2 μN. For NCD, the corresponding changes were from 77° to 37° and from 2.2 μN to 3.4 μN. An increasing trend was also observed for the friction coefficient (Fig. 4), albeit smaller than the change in the BEM-calculated capillary force. As discussed earlier, this inconsistency may be attributed to the imprecision of the capillary force estimates. The trend in increasing capillary force estimated here from BEM and experiment is also in line with the analytical and experimental capillary adhesion model developed earlier for a single-asperity contact [51]. The relative humidity effect and the hydrophilicity effect are dominated, respectively, by the water supply capacity of the environment and the water storage capacity at the interface. Combined, they determine the contribution of capillary condensation to the friction response in microscopic multi-asperity contacts.

4. Summary and conclusion

In this study, we have investigated how electrochemical corrosion influences the surface hydrophilicity of MCD and NCD surfaces, and how capillary adhesion due to water condensation contributes to friction force at multi-asperity contacts on non-corroded and corroded diamond surfaces in water-immersed, low RH, and humid air conditions. To quantify the interfacial capillary adhesion at the contact interfaces and its effect on the friction response, the capillary forces between a colloidal microsphere and rough PCD films before and after electrochemical corrosion were estimated for the different conditions from both microscopic lateral force experiments and elastoplastic BEM contact calculations. In the latter, the elastic solid contact area and capillary-wetted area were estimated based on the interfacial gaps as affected by the ambient humidity and the surface hydrophilicity. The results indicate strongly that the observed increase in friction force on corroded PCD surfaces is governed by enhanced capillary adhesion at the multi-asperity tribological interface, as affected by electrochemical corrosion (causing an increase in surface hydrophilicity) and by increasing environmental humidity. Compared to MCD, NCD surfaces, which have a greater intercrystallite boundaries area, experienced more intense electrochemical corrosion and showed higher observed friction forces as a result of smaller surface roughness and higher surface hydrophilicity. The enhanced capillary adhesive force contributes to the normal load and reduces the interfacial gap (increases the solid contact area), thus increasing friction force. These insights pave the way for better control over tribological properties in demanding high-tech applications.

CRediT authorship contribution statement

Chen Xiao: Conceptualization, Methodology, Validation, Formal analysis, Data curation, Writing – original draft. **Liang Peng:** Methodology, Formal analysis, Data curation, Writing – original draft. **Cyrian Leriche:** Formal analysis, Data curation, Writing – original draft. **Feng-Chun Hsia:** Formal analysis, Writing – review & editing. **Bart Weber:** Writing – review & editing, Funding acquisition. **Steve Franklin:** Conceptualization, Supervision, Formal analysis, Writing – review & editing, Funding acquisition.

Declaration of competing interest

The authors declare that they have no known competing financial interests or personal relationships that could have appeared to influence the work reported in this paper.

Acknowledgements

This work has been carried out at the Advanced Research Center for Nanolithography (ARCNL), a public-private partnership of the University of Amsterdam (UvA), the Vrije Universiteit Amsterdam (VU), the Netherlands Organisation for Scientific Research (now) and the semiconductor equipment manufacturer ASML. B.W. acknowledges funding from the NWO VENI grant No. VI.Veni.192.177.

Appendix A. Supplementary data

Supplementary data to this article can be found online at https://doi.org/10.1016/j.carbon.2023.01.050.

References

[1] Y.V. Pleskov, Electrochemistry of diamond: a review, Russ. J. Electrochem. 38 (2002) 1275–1291.

[2] C. Xiao, F.C. Hsia, A. Sutton-Cook, B. Weber, S. Franklin, Polishing of polycrystalline diamond using synergies between chemical and mechanical inputs: a review of mechanisms and processes, Carbon 196 (2022) 29–48.

[3] H.A. Ching, D. Choudhury, M.J. Nine, N.A.A. Osman, Effects of surface coating on reducing friction and wear of orthopaedic implants, Sci. Technol. Adv. Mater. 15 (2014), 014402.

[4] M. Amaral, A. Dias, P. Gomes, M. Lopes, R. Silva, J. Santos, M. Fernandes, Nanocrystalline diamond: in vitro biocompatibility assessment by MG63 and human bone marrow cells cultures, J. Biomed. Mater. Res. A 87 (2008) 91–99.

[5] A.M. Schrand, S.A.C. Hens, O.A. Shenderova, Nanodiamond particles: properties and perspectives for bioapplications, Crit. Rev. Solid State Mater. Sci. 34 (2009) 18–74.

[6] B. Lingwall, T. Sexton, C. Cooley, Polycrystalline diamond bearing testing for marine hydrokinetic application, Wear 302 (2013) 1514–1519.

[7] O. Auciello, S. Pacheco, A.V. Sumant, C. Gudeman, S. Sampath, A. Datta, et al., Are diamonds a MEMS'best friend? IEEE Microw. Mag. 8 (2007) 61–75.

[8] T. Bautze, S. Mandal, O.A. Williams, P. Rodiere, T. Meunier, C. Bäuerle, Superconducting nano-mechanical diamond resonators, Carbon 72 (2014) 100–105.

[9] P. Ashcheulov, R. Škoda, J. Škarohlíd, A. Taylor, L. Fekete, F. Fendrych, et al., Thin polycrystalline diamond films protecting zirconium alloys surfaces: from technology to layer analysis and application in nuclear facilities, Appl. Surf. Sci. 359 (2015) 621–628.

[10] Q. Chang, Colloid and Interface Chemistry for Water Quality Control, Academic Press, 2016.

[11] F.C. Hsia, S. Franklin, P. Audebert, A.M. Brouwer, D. Bonn, B. Weber, Rougher is more slippery: how adhesive friction decreases with increasing surface roughness due to the suppression of capillary adhesion, Phys. Rev. Res. 3 (4) (2021), 043204.

[12] S. Kwon, B. Kim, S. An, W. Lee, H.Y. Kwak, W. Jhe, Adhesive force measurement of steady-state water nano-meniscus: effective surface tension at nanoscale, Sci. Rep. 8 (2018) 1–7.

[13] T. Gao, K. Zhang, X. Liu, K. Liu, J. Ye, Linking macroscale frictional properties to nanoscale water capillary bridges, Tribol. Int. 174 (2022), 107696.

[14] M. Lee, B. Kim, J. Kim, W. Jhe, Noncontact friction via capillary shear interaction at nanoscale, Nat. Commun. 6 (2015) 1–6.

[15] L. Chen, D. Ngo, J. Luo, Y. Gong, C. Xiao, X. He, et al., Dependence of water adsorption on the surface structure of silicon wafers aged under different environmental conditions, Phys. Chem. Chem. Phys. 21 (2019) 26041–26048.

[16] C. Xiao, P. Shi, W. Yan, L. Chen, L. Qian, S.H. Kim, Thickness and structure of adsorbed water layer and effects on adhesion and friction at nanoasperity contact, Colloid. Interfaces 3 (2019) 55.

[17] I.L. Singer, H. Pollock, Fundamentals of Friction: Macroscopic and Microscopic Processes, Springer Science & Business Media, 2012.

[18] L. Chen, L. Qian, Role of interfacial water in adhesion, friction, and wear—a critical review, Friction 9 (2021) 1–28.

[19] L. Chen, J. Wen, P. Zhang, B. Yu, C. Chen, T. Ma, et al., Nanomanufacturing of silicon surface with a single atomic layer precision via mechanochemical reactions, Nat. Commun. 9 (2018) 1542.

[20] C.M. Mate, R.W. Carpick, Tribology on the Small Scale: a Modern Textbook on Friction, Lubrication, and Wear, Oxford University Press, 2019.

[21] E. Riedo, I. Palaci, C. Boragno, H. Brune, The 2/3 power law dependence of capillary force on normal load in nanoscopic friction, J. Chem. Phys. B 108 (2004) 5324–5328.

[22] L. Bocquet, E. Charlaix, S. Ciliberto, J. Crassous, Moisture-induced ageing in granular media and the kinetics of capillary condensation, Nature 396 (1998) 735–737.

[23] T.N. Rao, D. Tryk, K. Hashimoto, A. Fujishima, Band-edge movements of semiconducting diamond in aqueous electrolyte induced by anodic surface treatment, J. Electrochem. Soc. 146 (1999) 680.

[24] L. Kavan, Z.V. Zivcova, V. Petrak, O. Frank, P. Janda, H. Tarabkova, et al., Boron-doped diamond electrodes: electrochemical, atomic force microscopy and Raman study towards corrosion-modifications at nanoscale, Electrochim. Acta 179 (2015) 626–636.

[25] F.M. Elam, F.C. Hsia, S. van Vliet, R. Bliem, L. Yang, B. Weber, et al., The influence of corrosion on diamond-like carbon topography and friction at the nanoscale, Carbon 179 (2021) 590–599.

[26] O. Sharifahmadian, F. Mahboubi, S. Yazdani, Comparison between corrosion behaviour of DLC and N-DLC coatings deposited by DC-pulsed PACVD technique, Diam. Relat. Mater. 95 (2019) 60–70.

[27] W. Li, D. He, W. Ren, L. Wang, L. Shang, G. Zhang, Tribological behaviors of DLC films in sulfuric acid and sodium hydroxide solutions, Surf. Interface Anal. 52 (2020) 396–406.

[28] Y.V. Pleskov, New corrosion-resistant electrodes: synthetic diamond and diamond-based materials. The semiconductor and structure aspects—a review, Prot. Met. 42 (2006) 103–118.

[29] M.R. Nellist, Y. Chen, A. Mark, S. Gödrich, C. Stelling, J. Jiang, et al., Atomic force microscopy with nanoelectrode tips for high resolution electrochemical, nanoadhesion and nanoelectrical imaging, Nanotechnology 28 (2017), 095711.

[30] C. Xiao, F. Elam, S. van Vliet, R. Bliem, S. Lépinay, N. Shahidzadeh, et al., Intercrystallite boundaries dominate the electrochemical corrosion behavior of polycrystalline diamond, Carbon 200 (2022) 1–7.

[31] X. Wang, S.H. Kim, C. Chen, L. Chen, H. He, L. Qian, Humidity dependence of tribochemical wear of monocrystalline silicon, ACS Appl. Mater. Interfaces 7 (2015) 14785–14792.

[32] C. Chen, C. Xiao, X. Wang, P. Zhang, L. Chen, Y. Qi, et al., Role of water in the tribochemical removal of bare silicon, Appl. Surf. Sci. 390 (2016) 696–702.

[33] D. Niu, G. Tang, The effect of surface wettability on water vapor condensation in nanoscale, Sci. Rep. 6 (2016) 1–6.

[34] F.C. Hsia, C.C. Hsu, L. Peng, F.M. Elam, C. Xiao, S. Franklin, et al., Contribution of capillary adhesion to friction at macroscopic solid–solid interfaces, Phys. Rev. Appl. 17 (2022), 034034.

[35] S. Kim, D. Kim, J. Kim, S. An, W. Jhe, Direct evidence for curvature-dependent surface tension in capillary condensation: kelvin equation at molecular scale, Phys. Rev. X 8 (2018), 041046.

[36] N.V. Zarate, A.J. Harrison, J.D. Litster, S.P. Beaudoin, Effect of relative humidity on onset of capillary forces for rough surfaces, J. Colloid Interface Sci. 411 (2013) 265–272.

[37] A. Tiwari, J. Wang, B. Persson, Adhesion paradox: why adhesion is usually not observed for macroscopic solids, Phys. Rev. E 102 (4) (2020), 042803.

[38] L. Pastewka, M.O. Robbins, Contact between rough surfaces and a criterion for macroscopic adhesion, Proc. Natl. Acad. Sci. USA 111 (9) (2014) 3298–3303.

[39] B. Persson, Capillary adhesion between elastic solids with randomly rough surfaces, J. Phys. Condens. Matter 20 (2008), 315007.

[40] Y. Liu, S. Mukherjee, N. Nishimura, M. Schanz, W. Ye, A. Sutradhar, et al., Recent advances and emerging applications of the boundary element method, Appl. Mech. Rev. 64 (2011), 030802.

[41] M.H. Müser, W.B. Dapp, R. Bugnicourt, P. Sainsot, N. Lesaffre, T.A. Lubrecht, et al., Meeting the contact-mechanics challenge, Tribol. Lett. 65 (2017) 1–18.

[42] J. Hu, Y. Chou, R. Thompson, J. Burgess, S. Street, Characterizations of nano-crystalline diamond coating cutting tools, Surf. Coat. Technol. 202 (2007) 1113–1117.

[43] D.B. Asay, S.H. Kim, Evolution of the adsorbed water layer structure on silicon oxide at room temperature, J. Phys. Chem. B 109 (2005) 16760–16763.

[44] F.P. Bowden, F.P. Bowden, D. Tabor, The Friction and Lubrication of Solids, Oxford university press, 2001.

[45] X. He, Z. Liu, L.B. Ripley, V.L. Swensen, I.J. Griffin-Wiesner, B.R. Gulner, et al., Empirical relationship between interfacial shear stress and contact pressure in micro-and macro-scale friction, Tribol. Int. 155 (2021), 106780.

[46] M. Bartosik, L. Kormos, L. Flajsman, R. Kalousek, J. Mach, Z. Liskova, et al., Nanometer-sized water bridge and pull-off force in AFM at different relative humidities: reproducibility measurement and model based on surface tension change, J. Phys. Chem. B 121 (2017) 610–619.

[47] L. Chen, X. He, H. Liu, L. Qian, S.H. Kim, Water adsorption on hydrophilic and hydrophobic surfaces of silicon, J. Phys. Chem. C 122 (2018) 11385–11391.

[48] K. Jinesh, J. Frenken, Capillary condensation in atomic scale friction: how water acts like a glue, Phys. Rev. Lett. 96 (2006), 166103.

[49] M. Jiang, H. Yu, X. Li, S. Lu, X. Hu, Thermal oxidation induced high electrochemical activity of boron-doped nanocrystalline diamond electrodes, Electrochim. Acta 258 (2017) 61–70.

[50] E. Hsiao, M.J. Marino, S.H. Kim, Effects of gas adsorption isotherm and liquid contact angle on capillary force for sphere-on-flat and cone-on-flat geometries, J. Colloid Interface Sci. 352 (2) (2010) 549–557.

[51] C. Xiao, C. Chen, Y. Yao, H. Liu, L. Chen, L. Qian, et al., Nanoasperity adhesion of the silicon surface in humid air: the roles of surface chemistry and oxidized layer structures, Langmuir 36 (2020) 5483–5491.